CrossMark

High Power Laser Science and Engineering, (2023), Vol. 11, e26, 6 pages.
doi:10.1017/hpl.2023.25

HIGH POWER LASER SCIENCE AND ENGINEERING

RESEARCH ARTICLE

Collimated gamma beams with high peak flux driven by laser-accelerated electrons

Lulin Fan[1,2,†], Tongjun Xu[1,†], Shun Li[1], Zhangli Xu[3], Jiancai Xu[1], Jianqiang Zhu[1], Baifei Shen[1,3], and Liangliang Ji[1]

[1] *State Key Laboratory of High Field Laser Physics and CAS Center for Excellence in Ultra-intense Laser Science, Shanghai Institute of Optics and Fine Mechanics, Chinese Academy of Sciences, Shanghai, China*

[2] *Center of Materials Science and Optoelectronics Engineering, University of Chinese Academy of Sciences, Beijing, China*

[3] *Department of Physics, Shanghai Normal University, Shanghai, China*

(Received 6 January 2023; revised 16 February 2023; accepted 9 March 2023)

Abstract

Laser-accelerated electrons are promising in producing gamma-photon beams of high peak flux for the study of nuclear photonics, obtaining copious positrons and exploring photon–photon interaction in vacuum. We report on the experimental generation of brilliant gamma-ray beams with not only high photon yield but also low divergence, based on picosecond laser-accelerated electrons. The 120 J 1 ps laser pulse drives self-modulated wakefield acceleration in a high-density gas jet and generates tens-of-MeV electrons with 26 nC and divergence as small as 1.51°. These collimated electrons produce gamma-ray photons through bremsstrahlung radiation when transversing a high-Z solid target. We design a high-energy-resolution Compton-scattering spectrometer and find that a total photon number of 2.2×10^9 is captured within an acceptance angle of 1.1° for photon energies up to 16 MeV. Comparison between the experimental results and Monte Carlo simulations illustrates that the photon beam inherits the small divergence from electrons, corresponding to a total photon number of 2.2×10^{11} and a divergence of 7.73°.

Keywords: bremsstrahlung; Compton scattering; gamma-ray beam; laser-electron acceleration spectrometer

1. Introduction

In recent years, laser-driven particle sources, such as electrons[1], ions[2] and neutrons[3], have been greatly developed due to their promising applications in high-energy density physics, nuclear physics, and cancer therapy treatment. Based on laser-accelerated electrons, gamma-ray radiations are also gaining increasing interest due to their ultra-high peak brilliance, short pulse duration and small beam size[4–7]. Such compact gamma-ray sources could pave the way for nuclear photonics, producing ultra-short neutron sources and medical isotopes[8], and radiography. In particular, the small beam size and large peak flux of the laser-generated gamma-ray sources can greatly improve the contrast and spatial resolution for nondestructive radiography compared to other approaches[9]. In strong-field quantum-electrodynamics, a promising approach to observe the Breit–Wheeler electron–positron pair production[10] in the linear or nonlinear regime is to collide laser-driven gamma photons with superintense lasers[11], X-ray radiations[12] or with each other. This requires the gamma beams to be collimated, guaranteeing high photon density in the collision region.

There are three main mechanisms to generate gamma-ray beams based on laser-driven energetic electrons in experiments: betatron radiation[13], inverse Compton scattering (ICS)[14,15] and bremsstrahlung radiation[4,5,16,17]. In general, betatron radiation produces gamma rays with photon energies from hundreds of keV to MeV when electrons oscillate in the laser-driven plasma bubble field. In ICS, the number of photons obtained by laser photons scattered by high-energy electrons is usually at the 10^7 level[18], with photon energies up to several tens of MeV and good beam collimation. On the other hand, copious gamma photons can be produced when energetic electrons collide with high atomic-number nuclei through bremsstrahlung radiation. In this case, the

Correspondence to: Tongjun Xu and Liangliang Ji, State Key Laboratory of High Field Laser Physics and CAS Center for Excellence in Ultra-intense Laser Science, Shanghai Institute of Optics and Fine Mechanics, Chinese Academy of Sciences, Shanghai 201800, China. Email: tjxu@siom.ac.cn (T. Xu); jill@siom.ac.cn (L. Ji)

[†]These authors contributed equally to this work.

© The Author(s), 2023. Published by Cambridge University Press in association with Chinese Laser Press. This is an Open Access article, distributed under the terms of the Creative Commons Attribution licence (http://creativecommons.org/licenses/by/4.0), which permits unrestricted re-use, distribution and reproduction, provided the original article is properly cited.

https://doi.org/10.1017/hpl.2023.25 Published online by Cambridge University Press

maximum energy of the gamma photon is comparable to the maximum electron energy. It is advantageous for producing large photon numbers, up to 3.2×10^{10}, with a femtosecond laser[17] .

A key to increase the photon yield in bremsstrahlung radiation is enhancing the number of relativistic electrons in laser–plasma accelerations. For instance[16], using picosecond laser pulses of relatively high pulse energy, plasma wakefield acceleration in the self-modulated regime produces 7.5 nC electrons, hence inducing a photon number of 10^9 photons keV^{-1} Sr^{-1}. However, the divergence of bremsstrahlung gamma-ray beams is usually quite large (~several tens of degrees)[17] because of the scattering by the nucleus coulomb field.

In this work, to obtain high-yield low-divergence gamma sources, we first produce a collimated high-charge electron beam through picosecond laser-driven self-modulated wakefield acceleration (SM-LWFA). Then it is sent to a high-Z target. The bremsstrahlung gamma-ray photons are measured with a high-resolution Compton-scattering spectrometer (CSS). The latter contains a gradual magnetic field to improve the energy resolution. The measured spectra are reproduced with GEANT4 simulations, suggesting a total photon number of 2.2×10^{11} gamma photons (>0.3 MeV) within a divergence angle of 7.73°. Such gamma photons are advantageous in radiography, exploring nuclear photonics, strong-field quantum electrodynamics (QED) physics, etc.

2. Experimental setup

The experiment was carried out on the SG-II UP picosecond experimental platform[19] at the Shanghai Institute of Optics and Fine Mechanics (SIOM). A schematic diagram of the experiment is shown in Figure 1. A linearly polarized laser pulse with a pulse duration of $\tau_p = 1$ ps, a center wavelength of 1053 nm and an energy of 120 J was focused 600 μm above a pulsed nozzle that is employed to produce a high-density argon gas jet by an $f/2.8$ off-axis parabolic mirror. The focal spot has a full width at half maximum (FWHM) of 35 μm, reaching peak intensity of 3.1×10^{18} W/cm^2. The on-target laser field corresponds to a normalized laser amplitude $a \approx 2.3$, where $a = eE/m\omega c$, e and m are the electron charge and mass, E is the electric field, ω is the laser frequency and c is the speed of light in vacuum. The back pressure of the argon gas target in the experiment was 17–30 bar, and the optical interferometry of the laser–gas jet interaction indicated that the electron density reached a near-critical density region of (2–4) $\times 10^{20}$ cm^{-3}, corresponding to a plasma wavelength of $\lambda_p \approx 1.9$ μm. A 2 mm thick lead target was placed 2 mm behind the gas jet. When the laser-accelerated energetic electrons pass through the solid target, they are scattered by the nuclei and emit photons through bremsstrahlung radiation. Electron–positron pair creation through the Bethe–Heitler process[20] also occurs during the interaction process when the emitted photons further interact

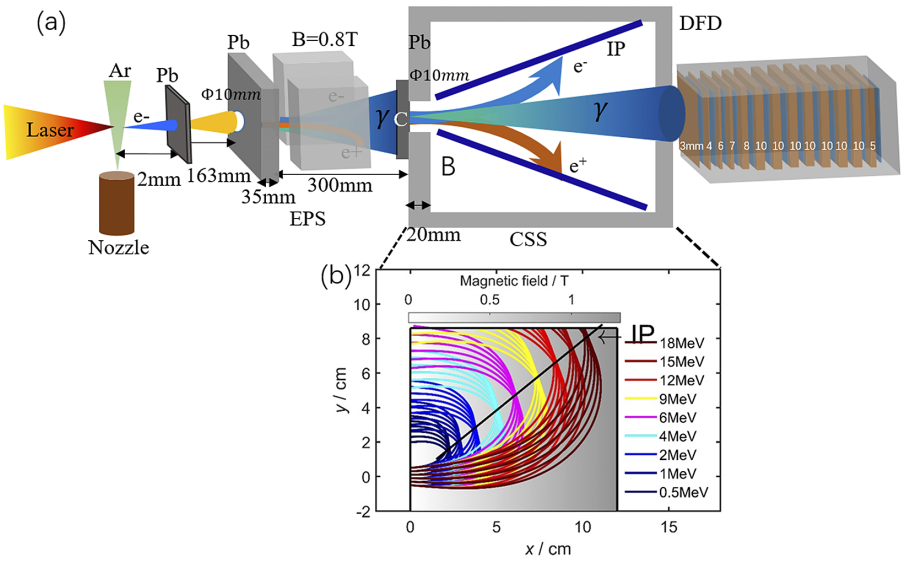

Figure 1. Schematic of the experimental setup. (a) A laser pulse propagates through an argon gas target, and energetic electrons are generated and collide with the 2 mm lead target located 2 mm behind the gas target to generate gamma-ray beams. An electron–positron spectrometer (EPS) with an aperture of 10 mm located 220 mm behind the lead target with an acceptance divergence angle of 2.86° is added to deflect the positrons and electrons and measure their energy spectra. The gamma-ray beam spectra are measured with a typical differential filtering detector (DFD) and a Compton-scattering spectrometer (CSS) with a gradual magnet, which increases linearly along the laser direction and fills the whole spectrometer. The converter target in the CSS is carbon with thickness of 2 mm. The CSS and DFD are added 500 mm behind the lead target, which has an acceptance divergence angle of 1.1°. (b) Trajectories of the converted electron beams dispersed in the gradual magnetic field. These trajectories represent incident electron beams with energies of 0.5–18 MeV. The converted electrons enter the magnetic field with different transverse positions of $[-5, 5]$ mm and different angles of $[-5°, 5°]$.

https://doi.org/10.1017/hpl.2023.25 Published online by Cambridge University Press

with nuclei. An electron–positron spectrometer (EPS) with the magnetic field of $B = 0.8$ T was added 220 mm behind the lead target to deflect the positrons and electrons and measure their energy spectra, which had an acceptance divergence angle of 2.86°. We chose Fuji BAS-SR (or BAS-TR) image plates (IPs) as the recording detector. The IPs were scanned using a GE Typhoon 7000 flatbed IP scanner[21].

One key aspect of our experiments is the measurement of the gamma-ray spectrum. Gamma-ray beams driven by laser-accelerated electrons are of short pulse duration, comparable to that of the laser pulse (~1 ps here). Conventional scintillation and semiconductor detectors are not applicable to resolve the energy spectrum of the gamma-ray flash since all photons reach the detector in a short instance, resulting in the integrated photon energy being the sum of all received gamma-ray beam energy. Therefore, methods such as Compton scattering[22,23], photonuclear activation[24,25] and differential filtering[26,27] are employed to detect ultrashort gamma-ray flashes. The neutron separation thresholds relevant to the photonuclear activation cover a wide energy range[25], while the attenuation coefficients are not so sensitive to gamma energy above 2 MeV in differential filtering[28]. Thus, their spectrum resolutions are limited, especially in the high-energy region.

In this experiment, we chose a differential filtering detector (DFD) and a CSS together to detect these photons. A typical CSS usually uses a uniform magnetic field profile[22] or a stepped magnetic field profile[23] to deflect the photon-induced electron–positron pairs. The latter employs a curved surface plate to improve the energy resolution. Instead, we apply a gradual magnetic field for CSS, which increases linearly along the laser direction and fills the whole spectrometer. Thus, it is capable of gathering the converted electrons with the same energy but different emitting angles together and enhances the energy resolution of the gamma-ray beam, as shown in Figure 1(b). There is the electron–positron pair effect in the MeV gamma-ray range. The influence of the electron–positron pair effect can be largely eliminated through their mutual cancellation by the adoption of a symmetrical design for the spectrometer such that the positron and electron spectra are measured simultaneously. Then the energy spectrum of gamma beams can be obtained from the corrected converted electron energy spectrum. The DFD is placed behind the CSS, which consists of 13 pieces of lead filters with dimensions of 2.5 cm × 2.5 cm and different thicknesses in the range of 3–10 mm, placed one by one in the beam path, as shown in Figure 1(a). The gamma-ray beam spectrum is calculated using the gamma-ray signal in each IP, considering the lead filter thickness and the attenuation coefficients of these 13 energy groups. We use equation $D_i = \Sigma_j^n R_{ij}\Phi_j, i = 1, 2, \cdots, 13$ to calculate the gamma-ray beam spectrum, where D_i represents the energy deposition on the ith channel detector, Φ_j is the photon number in the jth energy interval, n is the number of filters and R_{ij} is the energy deposition coefficient of photons in the jth energy interval on the ith filter. The CSS and DFD are added 500 mm behind the lead target, which has an acceptance divergence angle of 1.1°. In addition, the CSS and DFD are shielded by lead boxes with thicknesses of 1 and 2 cm to avoid the background radiation. Thus, the spectrometers measure the gamma-ray photon signal with low noise.

3. Experimental results and discussion

When a high-intensity $a > 1$ laser pulse with pulse duration τ_p larger than the plasma period λ_p/c propagates through an underdense plasma $n_e < n_c$, it undergoes self-focusing and drives plasma waves through the Raman forward scattering (RFS) and self-modulation instabilities[16]. The gas target is ionized simultaneously and a significant number of electrons are injected and accelerated. In our case, an argon cluster target with high density is employed to enhance the beam charge of energetic electrons from laser-driven electron acceleration[29]. The raw-data recorded by the EPS in Figure 2(a) show that the electron bunch has a broad energy spectrum with a cut-off energy of 80 MeV. After the deconvolution[30], the electron spectrum is plotted as shown in Figure 2(b). The electrons are first accelerated by the longitudinal field, while the transverse field leads to betatron-like oscillations of the off-axis electrons. This transverse electric field of the laser, when in near resonance with the betatron motion of the electrons, will in turn increase the transverse momentum of the electrons, which can be converted into longitudinal momentum via the $\boldsymbol{v}\times\boldsymbol{B}$ force. This process is analogous to the direct laser acceleration (DLA)[31]. The black line in Figure 2 represents the geometric mean value of the data. It is noted that the electrons accelerated in the plasma wave also undergo betatron oscillations about the laser axis due to the restoring

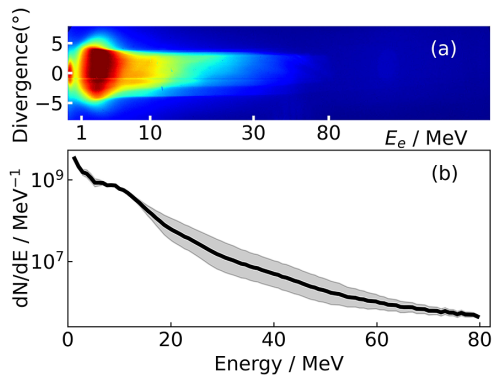

Figure 2. (a) Raw signal of the laser-accelerated electron beam recorded in the IP. (b) Extracted energy spectrum of the energetic electron beam. The black line represents the geometric mean value of the data of two shots. The shaded region represents uncertainty.

https://doi.org/10.1017/hpl.2023.25 Published online by Cambridge University Press

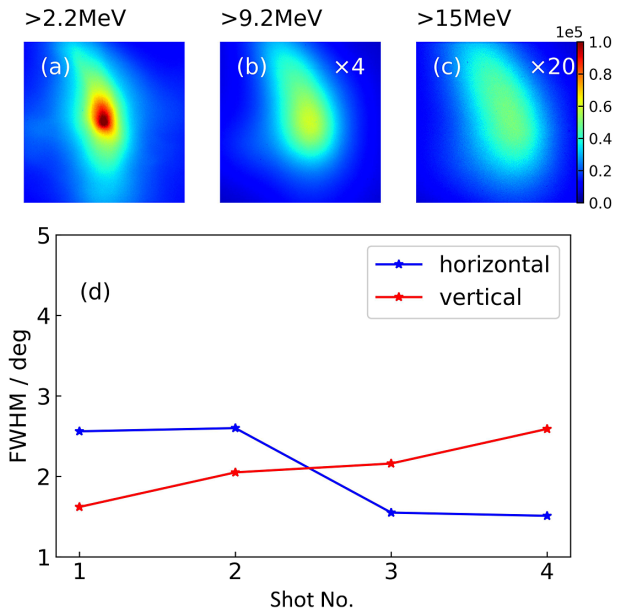

Figure 3. (a)–(c) Spatial distribution of the electron beam recorded in the IP corresponding to different energies, namely, $E > 2.2$ MeV, $E > 9.2$ MeV and $E > 15$ MeV. (d) Electron beam divergence angles of four continuous shots. The blue and red lines represent horizontal and vertical divergence angles, respectively.

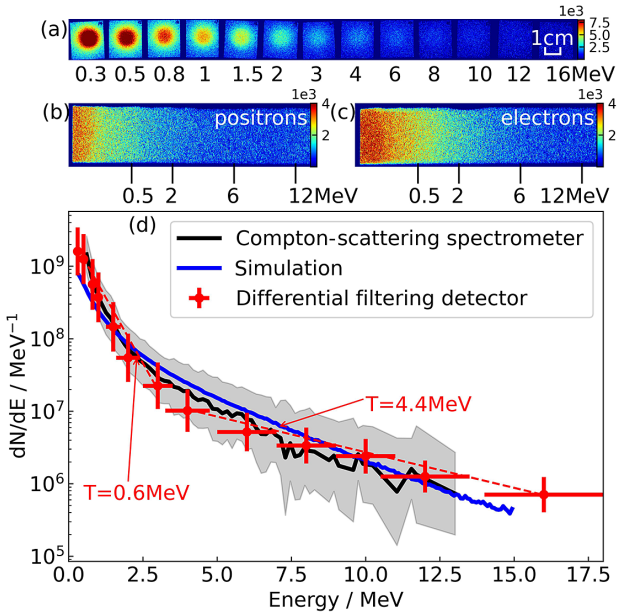

Figure 4. (a) Raw-data of the gamma-photon signal recorded by the DFD. Raw-data of positrons (b) and electrons (c) recorded by the CSS. (d) Experimental spectra from the CSS (black solid), the DFD (red cross) and GEANT4 simulation with the experimental electrons as input (blue solid), within the divergence angle of 1.1°. These horizontal error bars represent 13 energy intervals and the vertical error bars represent uncertainty for the DFD. The black line represents the geometric mean value of the data and the shaded region represents uncertainty for the CSS.

force of the ion column that forms behind the drive laser[16]. However, most of the radiation from betatron oscillations cannot pass through the thick lead target in the experiment.

Removing the lead target and spectrometers, a spatial high-energy electron beam analyzer (SHEEBA)[32] composed of Al plates and IPs is located 500 mm behind the argon target to detect the spatial distribution of the electrons. Figure 3(a) shows a spatial profile of the electrons with energy of more than 2.2 MeV, blocked by a 5-mm-thick Al plate in front. It has a Gaussian-type distribution with horizontal divergence of 1.51° and vertical divergence of 2.59° for shot 4. The spatial distribution of the electrons seems to be elliptic, almost the same direction as laser polarization, which could be attributed to the residual transverse momentum[16,33] that the electrons gain at the moment of ionization and/or to DLA[34,35]. The divergence angle of the electron beam increases while the energy increases from $E > 9.2$ MeV to $E > 15$ MeV, as shown in Figures 3(b) and 3(c). Electron beam divergence angles of four continuous shots show good stability in Figure 3(d), where the blue and red lines indicate the horizontal and vertical divergence angles, respectively. An electron beam charge of 26 nC is measured here, which is beneficial to the subsequent applications. Detailed analysis of the generated electron beams will appear elsewhere. Such high-charge electron beams have also been obtained by a picosecond-scale[31] kilojoule-class laser, where the total charge in the electron beams exceeds 700 nC and scales approximately linearly with the laser intensity.

These electrons with nC of charge and low divergence then collide with the 2-mm-thick lead target to generate gamma-ray photons through bremsstrahlung radiation. The EPS serves to remove the secondary electrons and positrons leaving the converting target here. The raw-data recorded by the DFD are shown in Figure 4(a) within the acceptance angle 1.1°. The spectrum of the gamma-ray beam shows a two-temperature structure (0.6 and 4.4 MeV). It should also be noticed that the gamma-ray signal on the sixth IP is still clear enough after penetrating a 3.8-cm-thick lead-layer. With a 3-mm-thick lead layer in front of the first IP in Figure 4(a) to block gamma-ray beams with energy lower than 0.3 MeV, a high total photon number of 2.2×10^9 is detected by the DFD. The raw-data of positrons and electrons recorded by the CSS are shown in Figures 4(b) and 4(c). The continuous gamma-ray beam spectrum of the geometric mean is shown in Figure 4(d) by a black line, which is in good agreement with the result from the DFD and has a higher energy resolution.

To model the gamma-ray generation process, a series of test particle simulations are carried out with the Monte Carlo code GEANT4[36]. The simulation includes several physical processes, such as bremsstrahlung, scattering, ionization, pair production, photoelectric effect and Compton scattering. A total of 10^7 electrons with the same energy and spatial distributions as the experimental measurement in Figures 2 and 3 impact a 2-mm-thick lead target. The electron source is considered to be point-like. The simulated gamma-ray

https://doi.org/10.1017/hpl.2023.25 Published online by Cambridge University Press

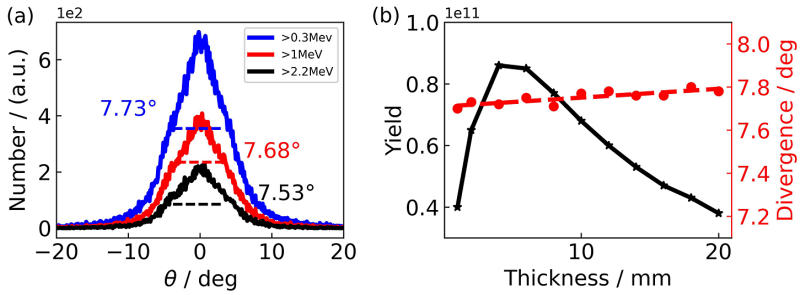

Figure 5. (a) The divergence of gamma-ray beam by GEANT4 simulation with energy > 0.3 MeV, > 1 MeV and > 2.2 MeV. (b) Gamma-ray photon (> 0.3 MeV) yields and divergence (FWHM) versus different lead thicknesses. The simulation is performed with the experimental electrons as input.

beam spectrum is shown by the blue line in Figure 4(d), and it is in good agreement with the experimental result, especially in the energy range above 2.5 MeV. The simulated temperatures of the gamma-ray beam within 1.1° are found to be 0.9 MeV for the low-energy part and 2.7 MeV for the high-energy part. The slight difference for the low-energy part from the experimental result has not been clarified, and further work is needed. Simulations also indicate that the produced gamma-ray source has an FWHM size of 433 μm at the emergent surface of the lead converter.

The simulated angular divergences of gamma-ray beams with different energies are summarized in Figure 5(a). It can be seen that the FWHM divergence of the gamma-ray beam of more than 0.3 MeV is only 7.73°, which is lower than the recent experimental results under commensurate laser conditions[16]. Considering that the gamma-ray beam has a 2D Gaussian distribution, the acceptance angle of 1.1° in the experiment means that only 1% of the photons are measured. Therefore, the total photon number generated in the experiment is estimated to be 2.2×10^{11} among the highest yield comparing to previous results[16,17,37] driven by laser-accelerated electrons. It is noted that the gamma-ray photon number could be further increased by raising the picosecond-scale laser energy[31]. The divergence of the gamma-ray beam decreases with the increase of energy, as shown in Figure 5(a). Overall, the gamma-ray beam with high yield and low divergence produced in our experiment could be a promising source for electron–positron production, radiography measurements in high energy density physics (HEDP) and inertial confinement fusion (ICF), and nuclear photonics.

The influence of thicknesses and the FWHM have also been studied by simulation, as shown in Figure 5(b). At the target thickness, the generated gamma-ray photon number increases due to continuous interaction between the electrons and the target. However, the energetic photons will be attenuated as the target thickness further increases. When these two processes reach a balance, the largest yield of gamma photons is obtained with the lead target thickness of 4 mm. The divergence angle of the gamma beams is basically unchanged while the target thickness increases.

4. Conclusion

In conclusion, we use a picosecond laser to generate electron beams with large charge and low divergence, and subsequently to generate gamma-ray beams with high yield and low divergence through bremsstrahlung radiation. A typical DFD and a specially designed high detection resolution CSS with a gradual magnetic field are used at the same time to detect the generated gamma-ray beams precisely. The gamma-ray beams have a total photon number of 2.2×10^{11}, size of 433 μm and divergence of 7.73°, which make them promising sources for photonuclear reaction and clinical applications. Future improvements on these sources can be done by using higher laser energies.

Acknowledgments

This work was supported by the National Key R&D Program of China (No. 2018YFA0404803), the National Natural Science Foundation of China (Nos. 12175299, 11905278, 11975302, and 11935008), the CAS Project for Young Scientists in Basic Research (No. YSBR060) and the Youth Innovation Promotion Association of Chinese Academy of Sciences (No. 2021242).

REFERENCES

1. A. J. Gonsalves, K. Nakamura, J. Daniels, C. Benedetti, C. Pieronek, T. C. H. de Raadt, S. Steinke, J. H. Bin, S. S. Bulanov, J. van Tilborg, C. G. R. Geddes, C. B. Schroeder, C. Toth, E. Esarey, K. Swanson, L. Fan-Chiang, G. Bagdasarov, N. Bobrova, V. Gasilov, G. Korn, P. Sasorov, and W. P. Leemans, Phys. Rev. Lett. **122**, 084801 (2019).
2. A. Macchi, M. Borghesi, and M. Passoni, Rev. Mod. Phys. **85**, 751 (2013).
3. M. M. Gunther, O. N. Rosmej, P. Tavana, M. Gyrdymov, A. Skobliakov, A. Kantsyrev, S. Zahter, N. G. Borisenko, A. Pukhov, and N. E. Andreev, Nat. Commun. **13**, 170 (2022).
4. Y. Glinec, J. Faure, L. L. Dain, S. Darbon, T. Hosokai, J. J. Santos, E. Lefebvre, J. P. Rousseau, F. Burgy, B. Mercier, and V. Malka, Phys. Rev. Lett. **94**, 025003 (2005).
5. A. Giulietti, N. Bourgeois, T. Ceccotti, X. Davoine, S. Dobosz, P. D'Oliveira, M. Galimberti, J. Galy, A. Gamucci, D.

https://doi.org/10.1017/hpl.2023.25 Published online by Cambridge University Press

Giulietti, L. A. Gizzi, D. J. Hamilton, E. Lefebvre, L. Labate, J. R. Marques, P. Monot, H. Popescu, F. Reau, G. Sarri, P. Tomassini, and P. Martin, Phys. Rev. Lett. **101**, 105002 (2008).
6. X.-B. Wang, G.-Y. Hu, Z.-M. Zhang, Y.-Q. Gu, B. Zhao, Y. Zuo, and J. Zheng, High Power Laser Sci. Eng. **8**, e34 (2020).
7. G. Sarri, D. J. Corvan, W. Schumaker, J. M. Cole, A. Di Piazza, H. Ahmed, C. Harvey, C. H. Keitel, K. Krushelnick, S. P. Mangles, Z. Najmudin, D. Symes, A. G. Thomas, M. Yeung, Z. Zhao, and M. Zepf, Phys. Rev. Lett. **113**, 224801 (2014).
8. S. Janek, R. Svensson, C. Jonsson, and A. Brahme, Phys. Med. Biol. **51**, 5769 (2006).
9. J. C. Kieffer, A. Krol, Z. Jiang, C. C. Chamberlain, E. Scalzetti, and Z. Ichalalene, Appl. Phys. B **74**, s75 (2014).
10. G. Breit and J. A. Wheeler, Phys. Rev. **46**, 1087 (1934).
11. D. L. Burke, R. C. Field, G. HortonSmith, J. E. Spencer, D. Walz, S. C. Berridge, W. M. Bugg, K. Shmakov, A. W. Weidemann, C. Bula, K. T. McDonald, E. J. Prebys, C. Bamber, S. J. Boege, T. Koffas, T. Kotseroglou, A. C. Melissinos, D. D. Meyerhofer, D. A. Reis, and W. Raggk, Phys. Rev. Lett. **79**, 1626 (1997).
12. T. Nousch, D. Seipt, B. Kämpfer, and A. I. Titov, Phys. Lett. B **755**, 162 (2016).
13. S. Cipiccia, M. R. Islam, B. Ersfeld, R. P. Shanks, E. Brunetti, G. Vieux, X. Yang, R. C. Issac, S. M. Wiggins, G. H. Welsh, M.-P. Anania, D. Maneuski, R. Montgomery, G. Smith, M. Hoek, D. J. Hamilton, N. R. C. Lemos, D. Symes, P. P. Rajeev, V. O. Shea, J. M. Dias, and D. A. Jaroszynski, Nat. Phys. **7**, 867 (2011).
14. S. Chen, N. D. Powers, I. Ghebregziabher, C. M. Maharjan, C. Liu, G. Golovin, S. Banerjee, J. Zhang, N. Cunningham, A. Moorti, S. Clarke, S. Pozzi, and D. P. Umstadter, Phys. Rev. Lett. **110**, 155003 (2013).
15. K. T. Phuoc, S. Corde, C. Thaury, V. Malka, A. Tafzi, J. P. Goddet, R. C. Shah, S. Sebban, and A. Rousse, Nat. Photonics **6**, 308 (2012).
16. N. Lemos, F. Albert, J. L. Shaw, D. Papp, R. Polanek, P. King, A. L. Milder, K. A. Marsh, A. Pak, B. B. Pollock, B. M. Hegelich, J. D. Moody, J. Park, R. Tommasini, G. J. Williams, H. Chen, and C. Joshi, Plasma Phys. Control. Fusion **60**, 054008 (2018).
17. S. Li, B. Shen, J. Xu, T. Xu, Y. Yu, J. Li, X. Lu, C. Wang, X. Wang, X. Liang, Y. Leng, R. Li, and Z. Xu, Phys. Plasmas **24**, 093104 (2017).
18. S. Corde, K. T. Phuoc, G. Lambert, R. Fitour, V. Malka, A. Rousse, A. Beck, and E. Lefebvre, Rev. Mod. Phys. **85**, 1 (2013).
19. J. Zhu, J. Zhu, X. Li, B. Zhu, W. Ma, X. Lu, W. Fan, Z. Liu, S. Zhou, G. Xu, G. Zhang, X. Xie, L. Yang, J. Wang, X. Ouyang, L. Wang, D. Li, P. Yang, Q. Fan, M. Sun, C. Liu, D. Liu, Y. Zhang, H. Tao, M. Sun, P. Zhu, B. Wang, Z. Jiao, L. Ren, D. Liu, X. Jiao, H. Huang, and Z. Lin, High Power Laser Sci. Eng. **6**, e55 (2018).
20. T. Xu, B. Shen, J. Xu, S. Li, Y. Yu, J. Li, X. Lu, C. Wang, X. Wang, X. Liang, Y. Leng, R. Li, and Z. Xu, Phys. Plasmas **23**, 033109 (2016).
21. G. J. Williams, B. R. Maddox, H. Chen, S. Kojima, and M. Millecchia, Rev. Sci. Instrum. **85**, 11E604 (2014).
22. D. J. Corvan, G. Sarri, and M. Zepf, Rev. Sci. Instrum. **85**, 065119 (2014).
23. Z.-C. Zhang, T. Yang, G.-Y. Hu, M.-T. Li, W. Luo, N. An, and J. Zheng, Matter Radiat. Extremes **6**, 014401 (2021).
24. W. P. Leemans, D. Rodgers, P. E. Catravas, C. G. R. Geddes, G. Fubiani, E. Esarey, B. A. Shadwick, R. Donahue, and A. Smith, Phys. Plasmas **8**, 2510 (2001).
25. M. M. Günther, K. Sonnabend, E. Brambrink, K. Vogt, V. Bagnoud, K. Harres, and M. Roth, Phys. Plasmas **18**, 083102 (2011).
26. C. D. Chen, J. A. King, M. H. Key, K. U. Akli, F. N. Beg, H. Chen, R. R. Freeman, A. Link, A. J. Mackinnon, A. G. MacPhee, P. K. Patel, M. Porkolab, R. B. Stephens, and L. D. Van Woerkom, Rev. Sci. Instrum. **79**, 10E305 (2008).
27. R. Nolte, R. Behrens, M. Schnurer, A. Rousse, and P. Ambrosi, Radiat. Protect. Dosim. **84**, 367 (1999).
28. J. H. Hubbell, H. A. Gimm, and I. Øverbø, J. Phys. Chem. Ref. Data **9**, 1023 (1980).
29. L. M. Chen, W. C. Yan, D. Z. Li, Z. D. Hu, L. Zhang, W. M. Wang, N. Hafz, J. Y. Mao, K. Huang, Y. Ma, J. R. Zhao, J. L. Ma, Y. T. Li, X. Lu, Z. M. Sheng, Z. Y. Wei, J. Gao, and J. Zhang, Sci. Rep. **3**, 1912 (2013).
30. T. Bonnet, M. Comet, D. Denis-Petit, F. Gobet, F. Hannachi, M. Tarisien, M. Versteegen, and M. M. Aleonard, Rev. Sci. Instrum. **84**, 103510 (2013).
31. J. L. Shaw, M. A. Romo-Gonzalez, N. Lemos, P. M. King, G. Bruhaug, K. G. Miller, C. Dorrer, B. Kruschwitz, L. Waxer, G. J. Williams, M. V. Ambat, M. M. McKie, M. D. Sinclair, W. B. Mori, C. Joshi, H. Chen, J. P. Palastro, F. Albert, and D. H. Froula, Sci. Rep. **11**, 7498 (2021).
32. M. Galimberti, A. Giulietti, D. Giulietti, and L. A. Gizzi, Rev. Sci. Instrum. **76**, 053303 (2005).
33. C. Thaury, E. Guillaume, S. Corde, R. Lehe, M. Le Bouteiller, K. Ta Phuoc, X. Davoine, J. M. Rax, A. Rousse, and V. Malka, Phys. Rev. Lett. **111**, 135002 (2013).
34. J. L. Shaw, N. Lemos, L. D. Amorim, N. Vafaei-Najafabadi, K. A. Marsh, F. S. Tsung, W. B. Mori, and C. Joshi, Phys. Rev. Lett. **118**, 064801 (2017).
35. S. P. Mangles, A. G. Thomas, M. C. Kaluza, O. Lundh, F. Lindau, A. Persson, F. S. Tsung, Z. Najmudin, W. B. Mori, C. G. Wahlstrom, and K. Krushelnick, Phys. Rev. Lett. **96**, 215001 (2006).
36. S. Agostinelli, J. Allison, K. Amako, J. Apostolakis, H. Araujo, P. Arce, M. Asai, D. Axen, S. Banerjee, G. Barrand, F. Behner, L. Bellagamba, J. Boudreau, L. Broglia, A. Brunengo, H. Burkhardt, S. Chauvie, J. Chuma, R. Chytracek, G. Cooperman, G. Cosmo, P. Degtyarenko, A. Dell'Acqua, G. Depaola, D. Dietrich, R. Enami, A. Feliciello, C. Ferguson, H. Fesefeldt, G. Folger, F. Foppiano, A. Forti, S. Garelli, S. Giani, R. Giannitrapani, D. Gibin, J. J. Gómez Cadenas, I. González, G. Gracia Abril, G. Greeniaus, W. Greiner, V. Grichine, A. Grossheim, S. Guatelli, P. Gumplinger, R. Hamatsu, K. Hashimoto, H. Hasui, A. Heikkinen, A. Howard, V. Ivanchenko, A. Johnson, F. W. Jones, J. Kallenbach, N. Kanaya, M. Kawabata, Y. Kawabata, M. Kawaguti, S. Kelner, P. Kent, A. Kimura, T. Kodama, R. Kokoulin, M. Kossov, H. Kurashige, E. Lamanna, T. Lampén, V. Lara, V. Lefebure, F. Lei, M. Liendl, W. Lockman, F. Longo, S. Magni, M. Maire, E. Medernach, K. Minamimoto, P. M. de Freitas, Y. Morita, K. Murakami, M. Nagamatu, R. Nartallo, P. Nieminen, T. Nishimura, K. Ohtsubo, M. Okamura, S. O'Neale, Y. Oohata, K. Paech, J. Perl, A. Pfeiffer, M. G. Pia, F. Ranjard, A. Rybin, S. Sadilov, E. Di Salvo, G. Santin, T. Sasaki, N. Savvas, Y. Sawada, S. Scherer, S. Sei, V. Sirotenko, D. Smith, N. Starkov, H. Stoecker, J. Sulkimo, M. Takahata, S. Tanaka, E. Tcherniaev, E. S. Tehrani, M. Tropeano, P. Truscott, H. Uno, L. Urban, P. Urban, M. Verderi, A. Walkden, W. Wander, H. Weber, J. P. Wellisch, T. Wenaus, D. C. Williams, D. Wright, T. Yamada, H. Yoshida, and D. Zschiesche, Nucl. Instrum. Methods Phys. Res. Sect. A **506**, 250 (2003).
37. A. Döpp, E. Guillaume, C. Thaury, A. Lifschitz, F. Sylla, J. P. Goddet, A. Tafzi, G. Iaquanello, T. Lefrou, P. Rousseau, E. Conejero, C. Ruiz, K. T. Phuoc, and V. Malka, Nucl. Instrum. Methods Phys. Res. Sect. A **830**, 515 (2016).

https://doi.org/10.1017/hpl.2023.25 Published online by Cambridge University Press